NANO LETTERS

Letter

pubs.acs.org/NanoLett

Size-Controlled Model Co Nanoparticle Catalysts for CO_2 Hydrogenation: Synthesis, Characterization, and Catalytic Reactions

Viacheslav Iablokov,[‡,†,#] Simon K. Beaumont,[†,#] Selim Alayoglu,[†,#] Vladimir V. Pushkarev,[†] Colin Specht,[†] Jinghua Gao,[⊥] A. Paul Alivisatos,[§,†] Norbert Kruse,[‡] and Gabor A. Somorjai*[,§,∥,†]

[†]Department of Chemistry, University of California Berkeley, Berkeley, California, United States

[‡]Université Libre de Bruxelles, Chimie Physique des Matériaux, Campus de la Plaine CP 243,B-1050 Bruxelles, Belgium

[§]Materials Sciences Division and [∥]Chemical Sciences Division, Lawrence Berkeley National Lab, Berkeley, California, United States

[⊥]Advanced Light Source, Lawrence Berkeley National Lab, Berkeley, California, United States

S *Supporting Information*

ABSTRACT: Model cobalt catalysts for CO_2 hydrogenation were prepared using colloidal chemistry. The turnover frequency at 6 bar and at 200−300 °C increased with cobalt nanoparticle size from 3 to 10 nm. It was demonstrated that near monodisperse nanoparticles in the size range of 3−10 nm could be generated without using trioctylphosphine oxide, a capping ligand that we demonstrate results in phosphorus being present on the metal surface and poisoning catalyst activity in our application.

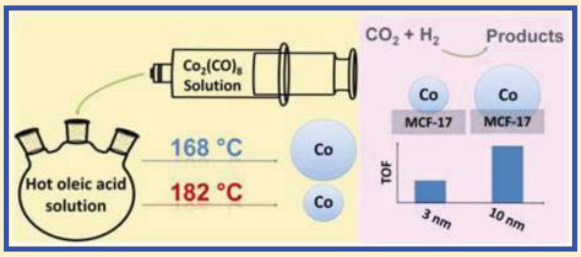

KEYWORDS: *Cobalt nanoparticles, CO_2 hydrogenation, heterogeneous catalysis, catalytic poisoning*

Cobalt-catalyzed processes and specifically the conversion of synthesis gas to hydrocarbons using cobalt (Co), Fischer−Tropsch synthesis, although long established,[1] have recently become a topic of renewed interest. This results from increased demand and declining fossil fuel reserves making both gas-to-liquid and biomass-to-liquid attractive routes to transportation fuels.[2] Especially when derived from biomass, the synthesis gas typically contains a significant fraction of CO_2, however studies on CO_2 hydrogenation and its catalytic mechanism on Co are much less well developed than the analogous reaction with CO.[3,4] Because of its environmental impact through the greenhouse effect, fixation of CO_2 by reaction (rather than simply capture and storage) also makes studying the possibility of Co-catalyzed CO_2 hydrogenation a topic of considerable interest.[4] Additionally, there is an important technical precedent in terms of producing desirable oxygenated products by incorporation of CO_2 in such reactions (important in producing synthetic fuels). In the case of classical Cu/ZnO catalyzed methanol production, Chinchen et al. demonstrated using isotopic labeling studies that it is CO_2, rather than CO, that is incorporated in the methanol produced.[5]

Few kinetic studies of the chemistry of Co-catalyzed CO_2 hydrogenation exist. In our laboratory the conversion of CO_2 to CH_4 was explored at atmospheric pressure in a batch reactor over high-purity Co foil,[6] subsequently Welder and co-workers also studied the hydrogenation of CO_2 over Co foils in a flow reactor.[7,8] Wetherbee and Bartholomew however have reported on the use of a Co/SiO_2 catalyst prepared by incipient wetness impregnation to obtain various kinetic parameters,[9] although this does not contain information at the atomic scale about the nature of the Co catalyst particles, and it is this problem that we now address.

In our laboratory size- and morphology-controlled nanoparticles, which are synthesized using colloidal techniques, have allowed the production of model catalysts via deposition within mesoporous silica supports. This is important because selectivity in multipath reactions has been found to vary with catalyst particle size and shape. In combination with powerful characterization techniques that provide atomic- and molecular-level information, these model nanoparticle catalysts have been employed in studying fundamental mechanistic questions in many key chemical reactions.[10] In the case of Co, size-controlled colloidal synthesis of metallic nanoparticles is particularly challenging, and few strategies exist for this purpose. Recently a number of strategies for the synthesis of monodisperse metallic Co nanoparticles have been proposed based on high-temperature decomposition of Co precursors in the presence of stabilizing agents. Murray and co-workers first showed that in the presence of trialkylphosphines and oleic acid, spherical nanoparticles could be produced from $CoCl_2$.[11] Shortly after it was also reported that roughly spherical 20 nm particles could be obtained by decomposition of $Co_2(CO)_8$ in solutions containing trioctylphosphine oxide (TOPO).[12] It has also been shown that organometallic Co complexes can be decomposed in the presence of some combination of acid and amine to yield nanoparticles which then organize into

Received: March 11, 2012
Revised: April 17, 2012
Published: May 2, 2012

nanorods.[13,14] Puntes et al. reported that the decomposition of $Co_2(CO)_8$ in the presence of oleic acid and TOPO provided a method to obtain size-controlled Co nanoparticles between 10 and 16 nm.[15] After aging for a matter of minutes these were spherical structures, which grow from nanodisks formed in the initial fast nucleation stage of the reaction.[16] The role of the TOPO was believed to be in enabling size focusing by stabilizing the process of transferring Co monomers from one nanoparticle to another,[16] and it was reported that in the absence of TOPO when only oleic acid is used as a stabilizing agent, a wide size distribution results.[15] Here we exploit this approach for producing model Co nanoparticle catalysts and show that it is possible to control size effectively below 10 nm using temperature as the controlling variable and also excluding TOPO, which we identify as a serious catalytic poison for CO_2 hydrogenation.

Phosphorus Poisoning of Catalytic Activity in CO_2 Hydrogenation. The role of TOPO in the preparation of Co nanoparticles is primarily attributed to its facilitating ripening and size focusing over time.[16] Although this is shown to be very effective for producing highly monodisperse 10−16 nm particles, in our experience it proved problematic for accessing much smaller Co nanoparticles, as might be expected for a 'ripening' effect. Since the role of such size focusing is to correct initial inhomogeneities, with the goal of accessing smaller particles reliably, we attempted to eliminate the need for such size focusing by careful control of the conditions in the initial seconds after injection of the Co precursor. Specifically rapid stirring and a larger flask than expected were utilized to ensure all the liquid is in close contact with the glass and external heating system, thus maintaining an even temperature. For ~10 nm particles as shown by the TEM images in Figure 1a, the synthesis could be conducted omitting the TOPO focusing agent and at slightly lower temperature with results almost comparable to that using TOPO (shown in Figure 1b for comparison). Side by side catalytic testing of these samples (Figure 1c) however demonstrates a key point concerning the importance of careful choice of colloidal synthesis strategies when preparing model catalysts. Although the morphology and size distributions appear very similar (Figure 1a,b), their reactivity is very markedly different. Under CO_2 hydrogenation reaction conditions, Co particles prepared using the alkylphosphine oxide and oleic acid were almost completely inert with regard to catalyzing the reaction, as compared to those prepared using only oleic acid stabilizer but still using $Co_2(CO)_8$ precursor.

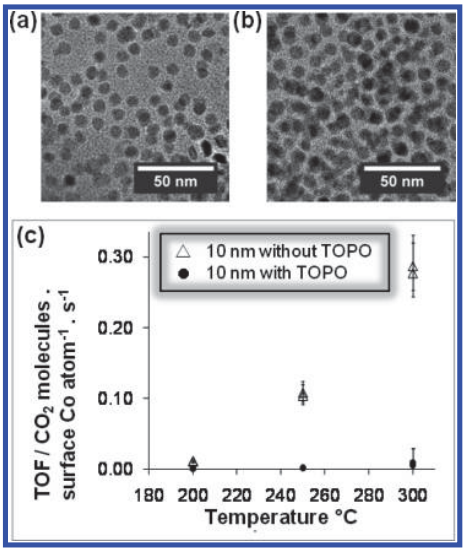

Figure 1. Showing TEM images of the 10 nm particles prepared using $Co_2(CO)_8$ precursor and (a) without TOPO or (b) using TOPO and (c) their corresponding activities for CO_2 hydrogenation reactions at various temperatures and 6 bar total pressure (CO_2:H_2:He 1:3:0.5). Errors are estimates based on uncertainty in Co surface area for each sample from the ICP-AES and TEM measurements; duplicate catalytic runs are shown on the graph for each condition.

Effect of Particle Size on CO_2 Hydrogenation. The approach outlined above of carefully controlling the homogeneity of the nucleation step to produce nanoparticles without a broad size distribution in the absence of TOPO as a focusing agent was, crucially for our purposes, possible to extend to reproducibly achieve smaller sizes between 3 and 10 nm (with oleic acid and $Co_2(CO)_8$ concentrations as detailed in the Supporting Information). Typical TEM images of the nanoparticles produced are shown in Figure 2, along with the obtained size distributions, which as can be seen are sufficiently monodisperse so as to not contain significant overlap. The different sizes were obtained by careful control of the temperature of the oleic acid in dichlorobenzene (DCB) solution into which the $Co_2(CO)_8$ was injected, and Figure 3 contains a plot of the obtained average particle size for a series of syntheses each conducted at a different temperature. It should be noted that lowering the temperature further gave a broad size distribution and that larger particles could not be achieved without changing other parameters.

By using size-controlled nanoparticles prepared according to this method of three discrete, nonoverlapping sizes (3, 7, and 10 nm) to prepare model catalysts by deposition in a mesoporous oxide support, it was then possible to explore the changes in the Co-catalyzed hydrogenation of carbon dioxide as the Co particle size was changed. The activity at a total pressure of 6 bar (H_2:CO_2:He 6:2:1) of the three different Co nanoparticle sizes is shown as a function of temperature in Figure 4. It is immediately obvious from the plotted TOF values that the smaller nanoparticles appear less active per surface Co site available. For the analogous CO hydrogenation using incipient wetness catalysts containing various sizes, it has been suggested particle sizes below ~7 nm in size are less active.[17] This is therefore a key point because it suggests the particle size behavior is common to both reactions—small particles have a lower activity than their larger counterparts. The lower activity of smaller particles in the CO hydrogenation reaction (typically studied using polydispersed catalysts of different loadings to give some control of particle size) has typically been attributed to a greater susceptibility to oxidation,[18] and it is known for other metals that this is the case for colloidally prepared nanoparticles, such as Ru or Rh.[19,20]

The turnover frequency (TOF) for the larger particles of around 0.1 CO_2 molecules (surface Co atom)$^{-1}$ s^{-1} at 250 °C is of a similar magnitude to the TOF data by Weatherbee and Bartholomew for their 15 wt % Co/SiO_2 catalyst prepared by incipient wetness (after extrapolation using the E_a values they report for reactant pressures of 1 and 11 bar).[9] However the E_a of around 75 ± 7 kJ mol^{-1} that is obtained for all particle sizes (by an Arrhenius fit of the data presented in Figure 4, see Supporting Information) appears lower than that reported, although direct comparison is not straightforward. The lack of

dx.doi.org/10.1021/nl300973b | Nano Lett. 2012, 12, 3091−3096

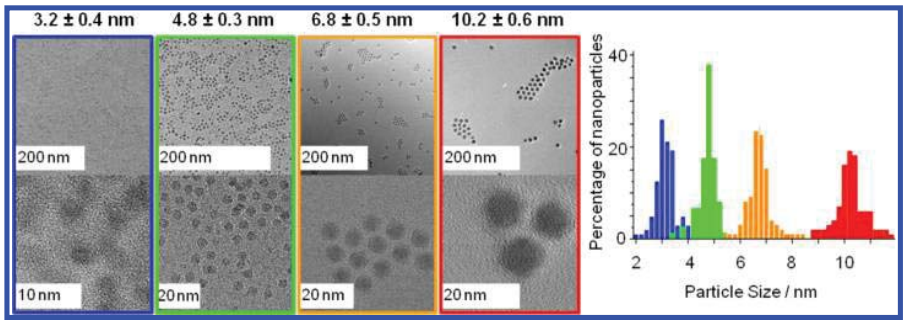

Figure 2. Typical TEM and HRTEM images of particles of four different sizes (3.2, 4.8, 6.8, and 10.2 nm) prepared without using TOPO and controlling particle size using variation in the temperature of the solution into which the $Co_2(CO)_8$ is injected and the corresponding particle size distributions obtained from counting 200−300 particles.

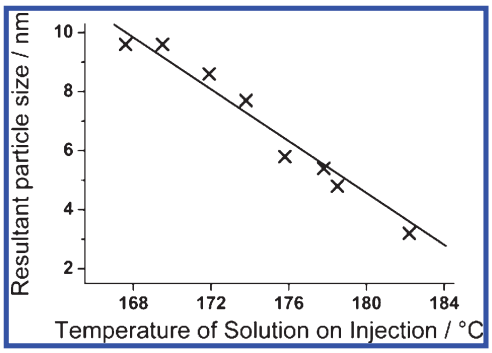

Figure 3. Plot of the resultant average particle size for a series of syntheses using different temperatures of the solution into which the $Co_2(CO)_8$ is injected.

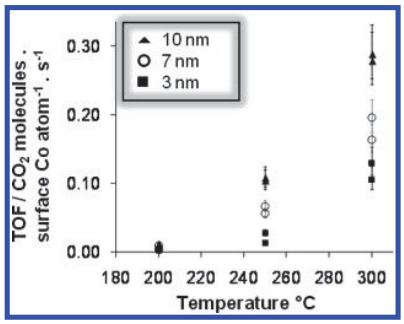

Figure 4. Showing activities for CO_2 hydrogenation reactions at various temperatures and 6 bar total pressure (CO_2:H_2:He 1:3:0.5) for 10, 7, and 3 nm Co nanoparticles prepared using TOPO free synthesis method to yield different particle sizes. Errors are estimates based on uncertainty in Co surface area for each sample from the ICP-AES and TEM measurements; duplicate catalytic runs are shown on the graph for each condition.

change in the apparent activation energy for different particle size is consistent with a change in the fraction of the surface available for reaction, for instance, as might result if metal surface required for reaction was lost due to oxidation. The TOF values reported on Co foils are all consistent with the reported value of 158 kJ mol^{-1}.[6,8] However the values found on Co/SiO_2 incipient wetness catalysts depend on both pressure and catalyst loading (which likely effects dispersion) and range between 79 kJ mol^{-1} at 0.07 bar reactant pressure and 3 wt % Co loading and 171 kJ mol^{-1} at 11 bar reactant pressure and 15 wt % loading.[9] There are therefore several plausible explanations for the differences, such as strong pressure dependence of the reaction kinetics and others, but it is clear that the activation energy on Co nanoparticles appears to often be significantly lower than on bulk metallic Co foils.

In terms of product distribution, no significant differences were seen for the different sized particles or the literature reports mentioned above. Methane and CO were the major products (selectivity to methane increasing from 20 to 40% across the temperature range explored) and traces of (<2 at. %) of C_2 products being seen at the highest temperature (300 °C).

Origin of Loss of Catalytic Activity for Samples Prepared Using TOPO. Since the reported TOF values are derived only from a TEM projected size, one possibility that could account for the difference would be that when TOPO is used, more organic material overall is used in the synthesis, and also there is a different type of molecule which may bind to the Co surface in a different manner. Either of these could result in more organic material being still present on the surface of the Co nanoparticle catalyst, even after careful washing and thermal pretreatment in H_2 at 450 °C and thus inhibiting the access of reactants. However, this possibility can be excluded by recourse to metal surface area measurements made on the catalyst using H_2/D_2 exchange immediately after the thermal pretreatment in H_2 and without exposure to air. These indicate that for the sample in Figure 1a containing no TOPO the surface area available to H_2 is 0.30 ± 0.04 m^2 g^{-1}, while for the sample containing TOPO in Figure 1b the H_2 can access 0.42 ± 0.06 m^2 g^{-1}. Since the catalysts are of similar loading, it is clear that less access to the Co surface is not the cause of the much lower catalytic activity in the case of the samples prepared using the alkylphosphine oxide—the available area is very similar in both cases.

Despite the fact it is reported elsewhere that the TOPO could be removed by washing[12] and that we could not detect P by XPS (estimated detection limit in our case is around 2 wt %), we also investigated the possibility of its presence in the as prepared particles by deposition of a thick film on a Si wafer and subsequent SEM/energy dispersive X-ray spectroscopy (EDS) analysis. This did detect phosphorus was still present but with an atomic ratio of P:Co of 1:24. This however does not address the question of whether the phosphorus is in contact with the Co or just in accompanying residual material that was also cast onto the Si wafer. We therefore used single particle electron energy loss spectroscopy (EELS) to assess whether or not the P is on the nanoparticles. Although the P L-edge (onset around 135 eV) is a relatively weak feature,[21] it can be seen in Figure 5a in the gray spectrum recorded on a Co nanoparticle as compared to one recorded on the adjacent C

dx.doi.org/10.1021/nl300973b | Nano Lett. 2012, 12, 3091−3096

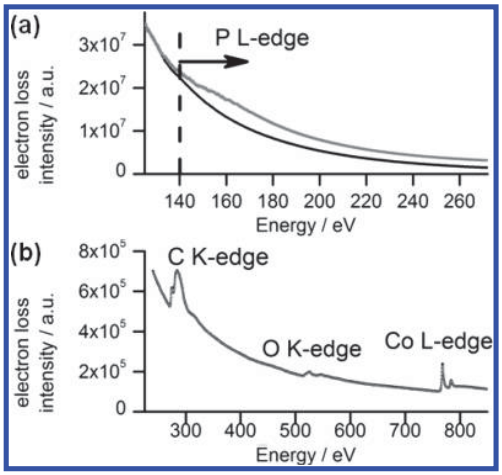

Figure 5. Typical EELS recorded on a single Co particle after deposition of the as prepared colloidal nanoparticles on a carbon film TEM grid. (a) The difference for the P L-edge region between the particle (gray) and the adjacent carbon film (black), the features or onset of the P L-edge being obvious by the difference above 140 eV. (b) Wide range EEL spectrum indicating the presence of other expected features and in particular the Co at 780 eV.

film (black), pointing toward the role of P in the poisoning of the catalyst. Figure 5b shows the EEL spectra for the region extending up to the Co L-edge recorded on the Co nanoparticle, confirming the presence of Co in this spot.

If the diminished catalytic activity is attributable to the presence of small quantities of P, it must also be present after thermal treatment, as is used to prepare the nanoparticle catalyst. This is much harder to detect reliably as the only TEM grids able to withstand these conditions contain Si, which has a considerable overlap with the P L-edge in the EEL spectra. However, two approaches both point to the likely presence of the P on the nanoparticles after treatment—both are shown in Figure 6. The first is to take a spectrum of the Co nanoparticle and then compare to the spectrum of just the Si alone—the positions used and the spectra are shown in Figure 6a and the spectra in (b). By normalizing to obtain the same maxima in the Si signal, there is a clear overlap of the two spectra below the onset of the P L-edge at around 135 eV, above which the difference spectrum shows there is a continuous gap, just as would be expected for passing across the step-edge due to the presence of P. The second is to locate nanoparticles overhanging holes in the Si film, such as the one marked B in Figure 6a. The resulting spectrum is shown in Figure 6c in gray as compared to the background reference obtained directly over vacuum in black. Again features and a step edge around 140 eV are apparent. Both results indicate the presence of a small quantity of P on the Co nanoparticle even after the treatment in H_2.

One plausible role of such a poison is in making the catalyst surface less easily reduced/more susceptible to oxidation. To investigate this possibility, we studied the reducibility of the Co surface by acquiring NEXAFS spectra in situ under 1 atm H_2 over a series of temperatures. The spectra obtained for the 10 nm Co nanoparticle samples prepared with (gray) and without (black) TOPO are shown in Figure 7 at both 175 and 225 °C.

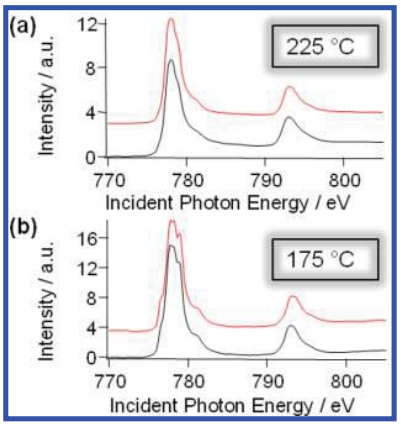

Figure 7. NEXAFS spectra of the Co L-edge acquired in situ during reduction of 2-D films of 10 nm Co nanoparticles deposited on silicon wafers (~50% coverage) in 1 bar H_2 using total electron yield detection and showing that both samples prepared with (red) and without (black) TOPO become reduced at very similar temperatures, being partially oxidized at 175 °C and almost fully reduced at 225 °C.

The oxidation states of the surface Co (typically a few nm[22] of depth) can be judged by comparing to reference spectra for Co^0 (metal), Co^{2+}, and Co^{3+},[23,24] as we have previously demonstrated.[25] The difference between oxidized and reduced Co is particularly distinct around the L_3 peak at 778 eV, which

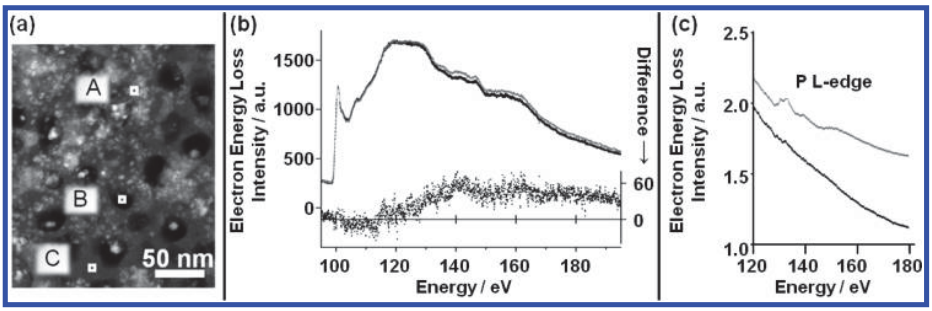

Figure 6. (a) TEM image showing Co nanoparticles prepared using TOPO and deposited on a holey Si film TEM grid and treated in H_2:He 4:1 for 2 h at 450 °C (exactly as the SiO_2 supported 3D catalysts are pretreated prior to use in CO_2 hydrogenation). Three points used to obtain the EELS spectra in (b) and (c) are indicated: (A) Co nanoparticles on Si film; (B) Co particles on edge of film over vacuum; and (C) Si film with no Co nanoparticles. (b) Comparison of EEL spectra in the P L-edge region recorded with (A, gray) and without (C, black) Co nanoparticles present. While the dominant features are those of the Si L-edge, the different spectrum shown beneath indicates clearly the onset of the P L-edge at around 140 eV. (c) Similar EEL spectrum recorded of the particles overhanging the vacuum (B, gray, Si signal absent) compared to the spectrum obtained of the vacuum alone (black).

dx.doi.org/10.1021/nl300973b | *Nano Lett.* 2012, 12, 3091−3096

is sharp for the metallic feature but has significant shoulders on either side (most noticeably for the higher photon energy side). Clearly in the case of both samples, reduction to an almost fully reduced Co^0 state occurs only on going from 175 to 225 °C, both being partial oxidized at the lower temperature. The absence of marked differences at either temperature indicates the poison has no strong effect on the electronic structure and reducibility. Since the Co remains available to adsorbing H_2 and there is no marked change on the overall surface electronic structure, the mechanism by which the P containing species poisons the surface with only small traces on P remaining on the surface remains a matter for subsequent study. However it should be noted that trace poisoning effects that extend much beyond the immediate radius of the poisoning atom are not unknown, sulfur on nickel being a well documented example.[26] For our purposes however the key point is that TOPO is not suitable for our use in preparing size-controlled model catalyst nanoparticles for CO_2 hydrogenation and must therefore be avoided.

In summary, careful control of the homogeneity of the nanoparticle synthesis reaction conditions using the 'hot injection' method to decompose a $Co_2(CO)_8$ precursor in the presence of oleic acid can produce near monodisperse Co nanoparticles over the 3−10 nm size range without using a TOPO focusing agent. The size obtained can be varied by careful control of the temperature of the hot oleic acid solution into which the Co precursor is injected. For samples of different sizes (prepared in the absence of TOPO), the TOF of CO_2 hydrogenation was found to be significantly higher on the larger nanoparticles and for the larger particles in reasonable agreement with the values reported elsewhere for an incipient wetness impregnation prepared catalyst. For all Co nanoparticle sizes, the CO_2 hydrogenation reaction product distribution was similar. The reaction produces mostly CO and CH_4 with traces of ethane and ethylene at high temperatures (300 °C). The presence of TOPO during nanoparticle synthesis had a negative impact on catalytic activity. SEM/EDAX and STEM/EELS indicate that small quantities of phosphorus atoms remain on the material after washing and catalyst pretreatment at 450 °C in H_2. H_2/D_2 exchange experiments indicate the poisoning effect is not due to reduced access for the reactants to the Co surface, and in situ NEXAFS spectroscopy shows there is no significant change to the reducibility or surface electronic structure of the sample caused by the phosphorus.

■ ASSOCIATED CONTENT

Ⓢ Supporting Information

Experimental methods; examples of temperature programmed reduction data; postreaction electron microscopy and H_2/D_2 titration of metal surface area for the 10 nm Co/MCF-17 catalyst; XRD and HRTEM data for the 4 and 10 nm nanoparticles; and Arrhenius plots of TOF data presented in Figure 4. This material is available free of charge via the Internet at http://pubs.acs.org.

■ AUTHOR INFORMATION

Corresponding Author

*E-mail: somorjai@berkeley.edu.

Author Contributions

#These authors contributed equally.

Notes

The authors declare no competing financial interest.

■ ACKNOWLEDGMENTS

This work was supported by the Director, Office of Science, Office of Basic Energy Sciences, Materials Sciences and Engineering Division, of the U.S. Department of Energy under contract no. DE-AC02-05CH11231. Nanoparticle imaging and spectroscopy were performed as a user project at the Molecular Foundry and National Center for Electron Microscopy, and NEXAFS was performed at the Advanced Light Source, Lawrence Berkeley National Laboratory, which is supported by the Office of Science, Office of Basic Energy Sciences, of the U.S. Department of Energy under contract no. DE-AC02-05CH11231. We gratefully acknowledge funding from Total, France. V.I. gratefully acknowledges a BRIC grant (Bureau des Relations Internationales et la Cooperation de l'ULB).

■ REFERENCES

(1) Fischer, F.; Tropsch, H. *Brennst.-Chem.* **1923**, *4*, 276−285.
(2) Khodakov, A. Y.; Chu, W.; Fongarland, P. *Chem. Rev.* **2007**, *107*, 1692−1744.
(3) Herranz, T.; Rojas, S.; Perez-Alonso, F. J.; Ojeda, A.; Terreros, P.; Fierro, J. L. G. *Appl. Catal., A* **2006**, *311*, 66−75.
(4) Yao, Y.; Hildebrandt, D.; Glasser, D.; Liu, X. *Ind. Eng. Chem. Res.* **2010**, *49*, 11061−11066.
(5) Chinchen, G. C.; Denny, P. J.; Parker, D. G.; Short, G. D.; Spencer, M. S.; Waugh, K.; Whan, D. A. *Abstracts of Papers of The American Chemical Society*; American Chemical Society: Washington, D.C., 1984; Vol. *29*, issue 5, pp 178−188.
(6) Lahtinen, J.; Anraku, T.; Somorjai, G. A. *Catal. Lett.* **1994**, *25*, 241−255.
(7) Frohlich, G.; Kestel, U.; Lojewska, J.; Lojewski, T.; Meyer, G.; Voss, M.; Borgmann, D.; Dziembaj, R.; Wedler, G. *Appl. Catal., A* **1996**, *134*, 1−19.
(8) Voss, M.; Frohlich, G.; Borgmann, D.; Wedler, G. *J. Catal.* **1999**, *187*, 348−357.
(9) Weatherbee, G. D.; Bartholomew, C. H. *J. Catal.* **1984**, *87*, 352−362.
(10) Tsung, C.-K.; Kuhn, J. N.; Huang, W.; Aliaga, C.; Hung, L.-I.; Somorjai, G. A.; Yang, P. *J. Am. Chem. Soc.* **2009**, *131*, 5816−5822.
(11) Sun, S. H.; Murray, C. B. *J. Appl. Phys.* **1999**, *85*, 4325−4330.
(12) Dinega, D. P.; Bawendi, M. G. *Angew. Chem., Int. Ed.* **1999**, *38*, 1788−1791.
(13) Dumestre, F.; Chaudret, B.; Amiens, C.; Fromen, M. C.; Casanove, M. J.; Renaud, P.; Zurcher, P. *Angew. Chem., Int. Ed.* **2002**, *41*, 4286−4289.
(14) Dumestre, F.; Chaudret, B.; Amiens, C.; Respaud, M.; Fejes, P.; Renaud, P.; Zurcher, P. *Angew. Chem., Int. Ed.* **2003**, *42*, 5213−5216.
(15) Puntes, V. F.; Krishnan, K. M.; Alivisatos, A. P. *Science* **2001**, *291*, 2115−2117.
(16) Puntes, V. F.; Zanchet, D.; Erdonmez, C. K.; Alivisatos, A. P. *J. Am. Chem. Soc.* **2002**, *124*, 12874−12880.
(17) Reuel, R. C.; Bartholomew, C. H. *J. Catal.* **1984**, *85*, 63−77.
(18) Wang, Z.; Skiles, S.; Yang, F.; Yan, Z.; Goodman, D. W. *Catal. Today* **2012**, *181*, 75−81.
(19) Joo, S. H.; Park, J. Y.; Renzas, J. R.; Butcher, D. R.; Huang, W.; Somorjai, G. A. *Nano Lett.* **2010**, *10*, 2709−2713.
(20) Grass, M. E.; Zhang, Y.; Butcher, D. R.; Park, J. Y.; Li, Y.; Bluhm, H.; Bratlie, K. M.; Zhang, T.; Somorjai, G. A. *Angew. Chem., Int. Ed.* **2008**, *47*, 8893−8896.
(21) Chen, T. C.; Qian, M.; Stoebe, T. G. *J. Phys.: Condens. Matter* **1999**, *11*, L341−L347.
(22) Stöhr, J. *NEXAFS*; Springer: Heidelberg, Germany, 1992; Vol. *25*.
(23) Morales, F.; de Groot, F. M. F.; Glatzel, P.; Kleimenov, E.; Bluhm, H.; Havecker, M.; Knop-Gericke, A.; Weckhuysen, B. M. *J. Phys. Chem. B* **2004**, *108*, 16201−16207.

(24) Kobayashi, M.; Hidai, S.; Niwa, H.; Harada, Y.; Oshima, M.; Horikawa, Y.; Tokushima, T.; Shin, S.; Nakamori, Y.; Aoki, T. *Phys. Chem. Chem. Phys.* **2009**, *11*, 8226−8230.
(25) Zheng, F.; Alayoglu, S.; Pushkarev, V. V.; Beaumont, S. K.; Specht, C.; Aksoy, F.; Liu, Z.; Guo, J.; Somorjai, G. A. *Catal. Today* **2012**, *182*, 54.
(26) Goodman, D. W. *Appl. Surf. Sci.* **1984**, *19*, 1−13.